

Power Scaling Laws and Near-Field Behaviors of Massive MIMO and Intelligent Reflecting Surfaces

Emil Björnson, *Senior Member, IEEE*, Luca Sanguinetti, *Senior Member, IEEE*

Abstract

Large arrays might be the solution to the capacity problems in wireless communications. The signal-to-noise ratio (SNR) grows linearly with the number of array elements N when using Massive MIMO receivers/relays. Moreover, intelligent reflecting surfaces (IRSs) have recently attracted attention since their SNR grows as N^2 , which seems like a major benefit. In this paper, we use a deterministic propagation model for a planar array of arbitrary size, to demonstrate that the mentioned SNR behaviors, and associated power scaling laws, only apply in the far-field. They cannot be used to study the regime where $N \rightarrow \infty$. We derive an exact channel gain expression that captures the near-field behavior and use it to revisit the power scaling laws. We derive new finite asymptotic SNR limits but also conclude that these are unlikely to be approached in practice. We further prove that an IRS setup cannot achieve a higher SNR than the corresponding Massive MIMO setups, despite its faster SNR growth. The IRS typically must have a much larger array size to achieve the same SNR. Finally, we show that an optimized IRS can be interpreted as a reconfigurable lens and that it is generally suboptimal to operate it as an “anomalous” mirror.

Index Terms

Intelligent reflecting surface, reconfigurable intelligent surface, metasurface, Massive MIMO, MIMO relays, power scaling law, near-field.

A preliminary version of this paper was presented at IEEE CAMSAP 2019 [1].

E. Björnson was supported by ELLIIT and the Wallenberg AI, Autonomous Systems and Software Program (WASP). L. Sanguinetti was partially supported by the University of Pisa under the PRA 2018-2019 Research Project CONCEPT, and by the Italian Ministry of Education and Research (MIUR) in the framework of the CrossLab project (Departments of Excellence).

E. Björnson is with the Department of Electrical Engineering (ISY), Linköping University, 58183 Linköping, Sweden (emil.bjornson@liu.se). L. Sanguinetti is with the Dipartimento di Ingegneria dell’Informazione, University of Pisa, 56122 Pisa, Italy (luca.sanguinetti@unipi.it).

I. INTRODUCTION

Massive MIMO (mMIMO) is the key physical layer technology in 5G [2]. In a nutshell, mMIMO uses a base station with many antennas (e.g., ≥ 64) to deliver large beamforming gains and perform spatial multiplexing of many users on the same time-frequency resource [3]–[5]. In this way, the spectral efficiency (SE) can be increased by, at least, an order of magnitude compared to 4G and mmWave communications can be enabled in mobile networks. Due to the success of mMIMO, it is expected that beyond 5G systems will make use of even larger arrays [6], which can be either active or passive.

The active arrays are essentially mMIMO transceivers but with many more antenna elements than what is conventionally considered. To make this clear, the research community has recently used new names to describe this category: *large intelligent surfaces* [7], *extremely large aperture arrays* [8], and *holographic MIMO* [9]. However, we will refer to it as mMIMO since asymptotically large arrays have been analyzed since the inception of mMIMO [3], [10], [11].

The passive arrays are large metasurfaces [12], [13] that are deployed somewhere in the propagation environment to support the transmission from a source to a destination by creating additional paths. A metasurface consists of many sub-wavelength-sized elements that each acts as a diffuse scatterer [12] but with the special feature of being able to adjust the phase and polarization. By controlling the phase-shifts of the individual elements, the metasurface can create a “reflected” beam in the desired direction [13]; the physics is the same as for beamforming with a phased array, except that the array then generates the signal locally. The concept of real-time controllable metasurfaces has recently received much attention and is called *intelligent reflecting surface (IRS)* [14], *software-controlled metasurface* [15], [16], and *reconfigurable intelligent surface* [17], [18]. We will call it IRS in this paper and will compare it with mMIMO relays, which are also deployed in between a source and destination to improve the propagation conditions; see [19]–[21] and reference therein for prior work on mMIMO relays.

A fundamental benefit of using large arrays is that the signal-to-noise ratio (SNR) grows with the number of elements N . In mMIMO setups, the SNR is proportional to N [10], [11], [19]–[21]. This implies that the transmit power needed to achieve a target SNR value during data transmission reduces as $1/N$, which is a so-called asymptotic power scaling law.¹ In contrast,

¹If one also reduces the transmit power in the channel acquisition phase, the power scaling law changes; we refer to [4], [10], [11] for details.

the SNR grows as N^2 when using an IRS [14], thus a more aggressive scaling law can be formulated where the transmit power is reduced as $1/N^2$ [14], [18], [22].

The main issue with the aforementioned SNR analyses and power scaling laws is that they are derived under an implicit assumption of far-field operation, which means that the direction and channel gain are approximately the same to all antennas in the array. However, since the array size grows with N , we will inevitably operate in the geometric near-field as $N \rightarrow \infty$. The near-field behavior of the SNR is uncertain. For example, several papers have studied the IRS behavior in the far- and near-field but as a specular reflector (an “anomalous” mirror) [18], [23]–[25], and made parallels to geometrical physics to support this conclusion. The conference version [1] of this paper was a first attempt to mathematically derive the near-field behavior in both the mMIMO and IRS setups, but the results are approximate since they relied on the propagation model from [7] that neglects polarization mismatches that appear over the array. Recently, [26], [27] provided numerical studies and discussions regarding the near-field behavior, but the results are approximate since polarization is neglected (as in [1], [7]). In [27], the effective areas of the elements are also assumed constant in the array, which is not the case in the near-field.

A. Contribution and Outline

In this paper, we begin by deriving a closed-form expression for the channel gain with a planar array of arbitrary size (see Sections II–III) and taking both varying polarization mismatches and effective areas of the element into account, which is necessary to rigorously study the near-field. We use this expression to mathematically derive the near-field and far-field behaviors in three key setups: conventional mMIMO, mMIMO relay, and IRS-supported communications. The setups are defined in Section IV, while the power scaling laws and near/far-field behaviors are uncovered in Section V. In particular, we explain under what conditions the SNR grows with N in the ways described above, and when we instead need to consider the different near-field behavior. The analysis shows that the far-field approximation is accurate for antenna arrays of practical interest but cannot be used to study their asymptotic limit as $N \rightarrow \infty$. We prove that an IRS can never achieve a higher SNR than the mMIMO setups when the array sizes are equal, despite the fact that the SNR sometimes grows as N^2 in the IRS setup. The case with different array sizes is then studied in Section VI. Next, in Section VII, we provide a geometric interpretation of an optimized IRS as a reconfigurable lens. This does not mean that the IRS

cannot operate as a specular reflector, but instead that this is not the SNR-maximizing way to operate it. Finally, the main results and conclusions are summarized in Section VIII.

B. Notation

Boldface lowercase letters, \mathbf{x} , denote column vectors and boldface uppercase letters, \mathbf{X} , denote matrices. The superscripts T , * , and H denote transpose, conjugate, and conjugate transpose, respectively. The $n \times n$ identity matrix is \mathbf{I}_n , $\text{mod}(\cdot, \cdot)$ indicates the modulo operation, and $\lfloor \cdot \rfloor$ rounds to the argument to the closest smaller integer. The multi-variate circularly symmetric complex Gaussian distribution with covariance matrix \mathbf{R} is denoted $\mathcal{N}_{\mathbb{C}}(\mathbf{0}, \mathbf{R})$. We define $\|\mathbf{x}\|$ the Frobenius norm of vector \mathbf{x} .

II. PRELIMINARIES

This paper analyzes the wireless propagation when using arrays of different sizes. We begin by considering the free-space propagation scenario shown in Fig. 1a, where an ideal isotropic transmit antenna sends a signal to a receive antenna located at distance d . Assume that the receive antenna is lossless, has an (effective) area A perpendicular to the direction of propagation, and has a polarization matching that of the transmitted signal. Then, from Friis' formula [28] the received power is

$$P_{\text{rx}} = \frac{A}{4\pi d^2} P_{\text{tx}} \quad (1)$$

where P_{tx} denotes the transmit power and

$$\beta_d = \frac{A}{4\pi d^2} \quad (2)$$

is the free-space channel gain, also known as pathloss. Note that it is given by the area of the receive antenna divided by the total surface area of a sphere with radius d . We use the subscript d in β_d to express that the channel gain is a function of d . Since the received power P_{rx} can never be higher than the transmit power P_{tx} (due to the law of energy conservation), it is evident that $\beta_d \in [0, 1]$. In most cases, β_d is much smaller than one, as we will now exemplify.

Example 1. *If the receive antenna is isotropic, its area is $A = \lambda^2/(4\pi)$ where $\lambda = c/fm$ is the wavelength and c is the speed of light. If the transmission has a carrier frequency of $f = 3 \text{ GHz}$, then $\lambda = 0.1 \text{ m}$. For propagation distances $d \in [2.5, 25] \text{ m}$, the channel gain β_d ranges from -40 dB to -60 dB . If the carrier frequency is increased to $f = 30 \text{ GHz}$, the antenna area becomes 100 times smaller and thus β_d will instead range from -60 dB to -80 dB for $d \in [2.5, 25] \text{ m}$.*

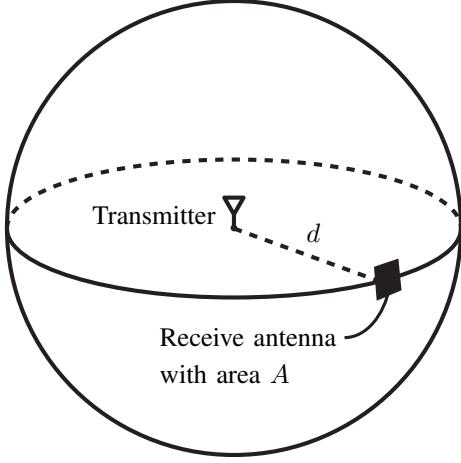
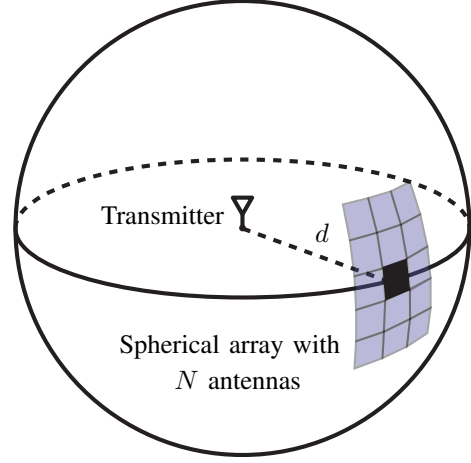
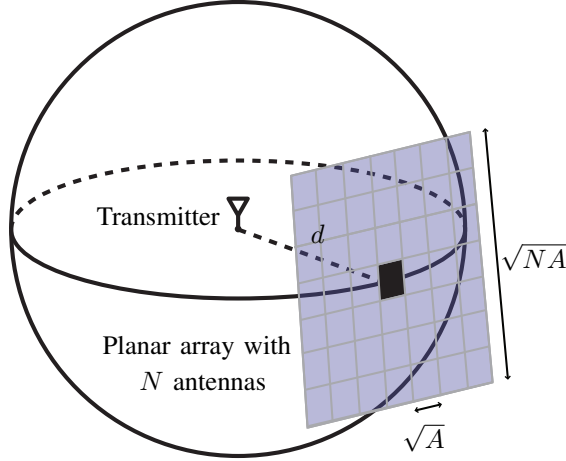
(a) One receive antenna with area A .(b) Spherical array with N equal-sized receive antennas.(c) Planar array with $\sqrt{N} \times \sqrt{N}$ equal-sized receive antennas.

Fig. 1: Examples of basic antenna scenarios.

A way to increase the channel gain in (2) is to make the receive antenna area larger. In particular, we can deploy N antennas of the same kind in an array. If they are deployed on the sphere in Fig. 1a and are non-overlapping, and if each antenna has a polarization that matches the locally received signal, the total received power is N times the value in (1):

$$P_{\text{rx}}^{\text{spheric-}N} = N P_{\text{rx}} = N \beta_d P_{\text{tx}}. \quad (3)$$

This setup is illustrated in Fig. 1b and the channel gain is $N \beta_d = \frac{NA}{4\pi d^2}$, which is proportional to the total antenna area NA . Clearly, no more than $NA = 4\pi d^2$ non-overlapping receive antennas can be deployed on the sphere in the way shown in Fig. 1b. In that case, $N \beta_d = 1$ and

$P_{\text{rx}}^{\text{spheric-}N} = P_{\text{tx}}$, so that all the transmitted power is received. Observe that very many antennas are needed to make this happen. Under the assumptions in Example 1, we need 10^4 antennas to cover the entire sphere for $d = 2.5$ m when communicating at $f = 3$ GHz, and 10^6 antennas for $d = 25$ m. Both values increase by 100 times when communicating at $f = 30$ GHz.

The linear growth with N in (3) is called an *array gain* and is the key motivating factor behind mMIMO communications using antenna arrays with a large (possibly infinite) number of antennas. A common statement in such systems is that the linear scaling holds true even in the asymptotic regime where $N \rightarrow \infty$ [3], [10], [11], [29]–[32]. This is clearly not possible since the total channel gain would be higher than one, thereby invalidating the law of energy consumption. At the same time, the analysis above has shown that a very large number of antennas is needed to receive all the transmitted power. Hence, the linear scaling might hold in practical mMIMO communications, even if thousands of antennas are used and the propagation distance is short. The aim of the next section is to revisit the asymptotic regime with practical planar antenna arrays and prove under what conditions the linear scaling is inaccurate or approximately correct. These results will be fundamental in Section V when studying the power scaling laws and near-field behaviors of different MIMO systems, including IRSs.

III. PLANAR ANTENNA ARRAYS

We now turn the attention to the planar array illustrated in Fig. 1c, particularly because such arrays are commonly used in practical mMIMO deployments [6]. The transmit antenna is at distance d from the center of the array. For notational convenience, we make the following assumption that will be considered in the remainder of this paper.

Assumption 1. *The planar array consists of N antennas that each has area A . The antennas have size $\sqrt{A} \times \sqrt{A}$ and are equally spaced on a $\sqrt{N} \times \sqrt{N}$ grid. The antennas are deployed edge-to-edge, thus the total area of the array is NA .*

These assumptions² are important when quantifying the channel gain, because the *effective* area of each receive antenna will depend on its physical location and rotation, with respect to the direction of the transmitter. An antenna that is fully perpendicular to the direction of

²Assumption 1 restricts N to be the square of an integer, but the analytical results of this paper only require a quadratic planar array with dimension $\sqrt{NA} \times \sqrt{NA}$. For a given array area NA , one can always adapt A to make N be the square of an integer.

propagation has effective area A , while other antennas have smaller effective areas. The antenna gain in a particular direction is determined by the effective area and polarization loss in that direction [33]. When the transmitter is in the so-called geometric near-field of the array, three fundamental properties must be taken into account: 1) the distance to the elements varies over the array; 2) the effective antenna areas vary since the element are seen from different angles; 3) the loss from polarization mismatch varies since the signals are received from different angles.

A. Exact Expression for the Channel Gain

The following lemma extends prior work in [33] and provides a general way of computing channel gains to each of the N antenna elements of a planar array.³

Lemma 1. *Consider a lossless isotropic antenna located at $\mathbf{p}_t = (x_t, y_t, d)$ that transmits a signal that has polarization in the Y direction when traveling in the Z direction. The receive antenna is located in the XY -plane, is centered at $\mathbf{p}_n = (x_n, y_n, 0)$, and has area $a \times a$. The free-space channel gain is*

$$\zeta_{\mathbf{p}_t, \mathbf{p}_n, a} = \frac{1}{4\pi} \sum_{x \in \mathcal{X}} \sum_{y \in \mathcal{Y}} \left(\frac{\frac{xy}{d^2}}{3 \left(\frac{y^2}{d^2} + 1 \right) \sqrt{\frac{x^2}{d^2} + \frac{y^2}{d^2} + 1}} + \frac{2}{3} \tan^{-1} \left(\frac{\frac{xy}{d^2}}{\sqrt{\frac{x^2}{d^2} + \frac{y^2}{d^2} + 1}} \right) \right) \quad (4)$$

where $\mathcal{X} = \{a/2 + x_n - x_t, a/2 - x_n + x_t\}$ and $\mathcal{Y} = \{a/2 + y_n - y_t, a/2 - y_n + y_t\}$.

Proof: The proof is given in Appendix A, where the impact of the three fundamental properties mentioned above is clearly pointed out. ■

We will use this general formula later in the paper. However, we first notice that a compact expression for the channel gain and thus the total received power can be obtained when the transmitter is centered in front of the planar array.

Corollary 1. *Under Assumption 1, when the transmitter is centered in front of the planar array, the received power is*

$$P_{\text{rx}}^{\text{planar-}N} = \alpha_{d,N} P_{\text{tx}} \quad (5)$$

where the total channel gain is

$$\alpha_{d,N} = \frac{N\beta_d}{3(N\beta_d\pi + 1)\sqrt{2N\beta_d\pi + 1}} + \frac{2}{3\pi} \tan^{-1} \left(\frac{N\beta_d\pi}{\sqrt{2N\beta_d\pi + 1}} \right) \quad (6)$$

with β_d given in (2).

³We disregard the mutual coupling effect in this paper, to focus on the asymptotic behaviors with ideal hardware.

Proof: This formula follows from Lemma 1 by setting $x_t = y_t = 0$, $x_n = y_n = 0$, and $a = \sqrt{NA}$, in which case $\mathcal{X} = \mathcal{Y} = \{\sqrt{NA}/2, \sqrt{NA}/2\}$. By replacing d with $\sqrt{A/(4\pi\beta_d)}$ and rearranging the terms, we obtain (6) from (4). ■

The channel gain in (6) is valid for arbitrarily large planar arrays, which is different from the models recently considered in [26], [27] that assume equal effective areas of all elements. The new expression supports the case when the transmitter is in the near-field of the array.⁴ We will now explore both far-field approximation and large-array limit appearing in the near-field.

B. Far-field Approximation and Large-array Limit

Suppose the planar array considered in Corollary 1 is in the far-field of the transmitter in the sense that $d \gg \sqrt{NA}$. In this case, $N\beta_d\pi + 1 \approx 1$ and $\sqrt{2N\beta_d\pi + 1} \approx 1$. By using the first-order Taylor approximation $\tan^{-1}(x) \approx x$, which is tight when the argument is close to zero (as is the case when $N\beta_d\pi$ is small), from (5) it follows that

$$P_{\text{rx}}^{\text{planar-}N} \approx \left(\frac{N\beta_d}{3} + \frac{2}{3\pi}N\beta_d\pi \right) P_{\text{tx}} = N\beta_d P_{\text{tx}} \quad (7)$$

which is equal to $P_{\text{rx}}^{\text{spheric-}N}$ in (3). Hence, for relatively small planar arrays, the received power is proportional to N . Both terms in (6) contribute to the result, but not equally much.

If N grows large, the far-field approximation is no longer valid and we instead notice that

$$\frac{N\beta_d}{3(N\beta_d\pi + 1)\sqrt{2N\beta_d\pi + 1}} \rightarrow 0, \quad (8)$$

$$\tan^{-1}\left(\frac{N\beta_d\pi}{\sqrt{2N\beta_d\pi + 1}}\right) \rightarrow \frac{\pi}{2}, \quad (9)$$

as $N \rightarrow \infty$. Hence, the received power in (5) saturates and has the asymptotic limit

$$P_{\text{rx}}^{\text{planar-}N} \rightarrow \frac{2}{3\pi} \frac{\pi}{2} P_{\text{tx}} = \frac{P_{\text{tx}}}{3} \quad \text{as } N \rightarrow \infty. \quad (10)$$

This value satisfies the law of energy conservation since only one third of the transmitted power is received. An intuitive explanation for why the limit is finite, although the array is infinitely large, is that each new receive antenna is deployed further away from the transmitter; the effective area (perpendicularly to the direction of propagation) becomes gradually smaller and the polarization loss also increases. The former effect is very important to model properly, otherwise there is no

⁴Note that we assume throughout this paper that $d \gg \lambda$, so the system does not operate in the reactive near-field of the transmit antenna (even if it is in the geometric near-field of the array). In fact, this assumption must be made to derive the expression in Lemma 1; see [33] for details.

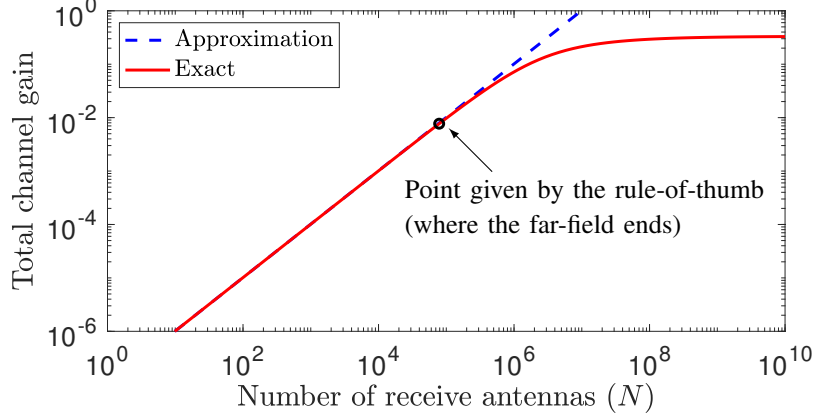


Fig. 2: The total channel gain $P_{\text{rx}}^{\text{planar-}N}/P_{\text{tx}}$ with a planar array with $\sqrt{N} \times \sqrt{N}$ equally spaced antennas. The setup defined in Example 1 is considered with $f = 3 \text{ GHz}$ and $d = 25 \text{ m}$.

limit and the law of energy conservation is invalidated. The latter effect is also of importance since the limit becomes $1/2$ if one neglects polarization losses, as was done in [1], [7].

From the above discussion, a natural question arises: *Will the received power grow linearly with N for practical array sizes, so that we can utilize the approximation in (7), or do we need to use the exact expression?* To answer this question, Fig. 2 shows the total channel gain $P_{\text{rx}}^{\text{planar-}N}/P_{\text{tx}} \in [0, 1]$ as a function of N , using either the exact expression in (5) or the far-field approximation in (7). We consider the setup defined in Example 1 with $f = 3 \text{ GHz}$ and $d = 25 \text{ m}$. The results of Fig. 2 show that nearly 10^5 antennas are needed before the approximation error is noticeable (above 5%), and 10^8 antennas are needed to approach the upper limit of $1/3$.

Remark 1. *The exact expression in (6) depends on $N\beta_d$, thus it is the total array area NA that matters and not the individual values of N and A . Hence, the results in this paper hold for any frequency band and choice of individual antenna areas, as long as the total area is the same. As the wavelength reduces, the area A typically shrinks and then more elements are needed to fill the same total array area.*

As a rule-of-thumb, the far-field approximation in (7) is accurate for all N satisfying $NA/10 \leq d^2$; the value of N that gives equality in this rule-of-thumb is indicated by a circle in Fig. 2. As the distance d increases or the carrier frequency increases, the maximum number of antennas that satisfies the rule-of-thumb grows quadratically. In conclusion, the far-field approximation is usually accurate and might be used to predict scaling behaviors, but the exact expression in

Corollary 1 is needed to study the asymptotic limit.

Remark 2. *The propagation models presented in this section are physically accurate, under the given assumptions, and will be used in the remainder of this paper. However, this does not mean that the assumptions are applicable in any conceivable practical setup. For example, there can be other antenna gains, other polarization directions, and channels consisting of multiple paths. We are not covering these generalizations since we focus on providing an intuitive exposition of the fundamental behaviors. Nevertheless, we claim that the properties that we expose will hold true also under other and/or more general conditions. The main difference is that additional scaling factors might appear in the SNR expressions and one might get summations of multiple expressions (representing multiple paths) of similar kinds as those in this paper.*

IV. THREE DIFFERENT MIMO SETUPS

Next, we describe the three different setups that are considered in this paper, which are all illustrated in Fig. 3. In the conventional mMIMO setup of Fig. 3a, a single-antenna source transmits a signal that is received by a planar array with N antennas, in the same form as in Fig. 1c. In the mMIMO relay setup shown in Fig. 3b, the same planar array receives the signal from the source and retransmits it to a single-antenna destination. In the IRS-aided setup in Fig. 3c, the planar array is replaced by an IRS with N passive elements that jointly “reflect” the incoming signal in a controllable manner. The signal comes from the source and is supposed to reach the destination. The IRS is intelligent in the sense that each of the N reflecting elements can control the individual phase of its diffusely reflected signal.

Line-of-sight (LoS) propagation is considered in all setups. Since the channels are deterministic and thus can be estimated arbitrarily well from pilot signals, perfect channel state information is assumed. Despite simple, the three setups in Fig. 3 are sufficient to develop the fundamental scaling laws and near-field behaviors (see Remark 2) and compare the setups.

A. Massive MIMO

In the LoS scenario, the deterministic flat-fading channel is represented by the vector $\mathbf{h} = [h_1, \dots, h_N]^T \in \mathbb{C}^N$, where $h_n = |h_n|e^{-j\phi_n}$ is the channel from the source to the n th receive antenna with $|h_n|^2 \in [0, 1]$ being the channel gain and $\phi_n \in [0, 2\pi]$ an arbitrary phase shift. In the uplink, the received signal $\mathbf{r}_{\text{mMIMO}} \in \mathbb{C}^N$ is

$$\mathbf{r}_{\text{mMIMO}} = \mathbf{h}\sqrt{P_{\text{tx}}}s + \mathbf{n} \quad (11)$$

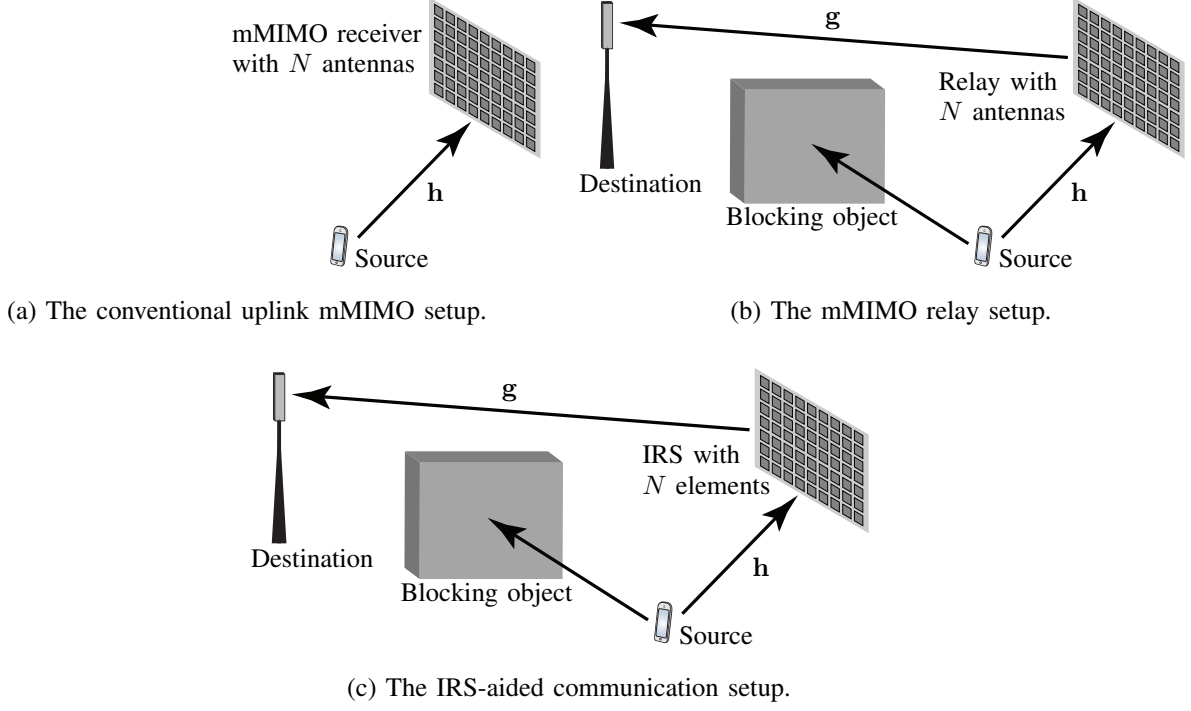


Fig. 3: Illustration of the three different MIMO setups compared in this paper.

where P_{tx} is the transmit power, s is the unit-norm information signal, and $\mathbf{n} \sim \mathcal{N}_{\mathbb{C}}(\mathbf{0}, \sigma^2 \mathbf{I}_N)$ is the independent receiver noise. Under the assumption of perfect channel knowledge, linear receiver processing is optimal [4], [34] and we let $\mathbf{v} \in \mathbb{C}^N$ denote the receive combining vector. It is well-known that the maximum SNR is achieved with maximum ratio (MR) combining, defined as $\mathbf{v} = \mathbf{h}^* / \|\mathbf{h}\|$ [4]. The SE is $\log_2(1 + \text{SNR}_{\text{mMIMO}})$ with

$$\text{SNR}_{\text{mMIMO}} = \frac{|\mathbf{v}^T \mathbf{h}|^2}{\|\mathbf{v}\|^2} \frac{P_{\text{tx}}}{\sigma^2} = \|\mathbf{h}\|^2 \frac{P_{\text{tx}}}{\sigma^2} = \left(\sum_{n=1}^N |h_n|^2 \right) \frac{P_{\text{tx}}}{\sigma^2}. \quad (12)$$

B. Massive MIMO Relay

The relay transmission takes place over two phases: 1) transmission from the source to the relay; 2) transmission from the relay to the destination. No direct link is present. Among the different relaying protocols (e.g., [35]–[37] among others), we consider the basic repetition-coded decode-and-forward protocol where equal time is allocated to the two phases. The first phase achieves the same SNR as in the mMIMO setup considered above. Therefore, the SE is $\frac{1}{2} \log_2(1 + \text{SNR}_{\text{mMIMO}})$ where $\text{SNR}_{\text{mMIMO}}$ is given in (12) and the pre-log factor represents the fact that each phase is allocated half of the time resources. In the second phase, the relay retransmits the signal s with power P_{relay} using a unit-norm precoding vector \mathbf{w} . The LoS channel

from the array to the destination is represented by the deterministic vector $\mathbf{g} = [g_1, \dots, g_N]^T \in \mathbb{C}^N$, where $g_n = |g_n|e^{-j\psi_n}$ represents the channel from the n th antenna to the receiver. The received signal $r_{\text{relay}} \in \mathbb{C}$ at the single-antenna destination is

$$r_{\text{relay}} = \mathbf{g}^T \mathbf{w} \sqrt{P_{\text{relay}}} s + n \quad (13)$$

where $n \sim \mathcal{N}_{\mathbb{C}}(0, \sigma^2)$ is the independent receiver noise. It is well-known that the SNR is maximized by MR precoding with $\mathbf{w} = \mathbf{g}^* / \|\mathbf{g}\|$ [4], which leads to

$$\text{SNR}_{\text{relay}} = \|\mathbf{g}\|^2 \frac{P_{\text{relay}}}{\sigma^2} = \left(\sum_{n=1}^N |g_n|^2 \right) \frac{P_{\text{relay}}}{\sigma^2}. \quad (14)$$

The SE of the end-to-end mMIMO relay channel is then given by the minimum of the two phases:

$$\text{SE}_{\text{relay}} = \frac{1}{2} \log_2 (1 + \min(\text{SNR}_{\text{mMIMO}}, \text{SNR}_{\text{relay}})). \quad (15)$$

C. Intelligent Reflecting Surface

The IRS-aided communication resembles the mMIMO relay case with the key difference that each element in the IRS scatters the incoming signal with a controllable phase-shift but without increasing its power. The received signal $r_{\text{IRS}} \in \mathbb{C}$ can be modeled as [26], [38]

$$r_{\text{IRS}} = \mathbf{g}^T \mathbf{\Theta} \mathbf{h} \sqrt{P_{\text{tx}}} s + n \quad (16)$$

where P_{tx} and s are the same as in the previous setups and $n \sim \mathcal{N}_{\mathbb{C}}(0, \sigma^2)$ is the noise at the receiver. The reflection properties are determined by the diagonal matrix

$$\mathbf{\Theta} = \mu \cdot \text{diag}(e^{j\theta_1}, \dots, e^{j\theta_N}) \quad (17)$$

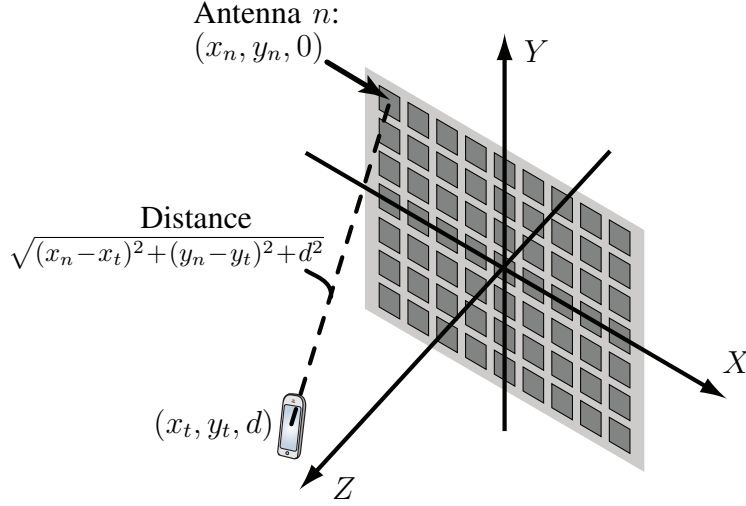
where $\mu \in (0, 1]$ is a fixed⁵ amplitude reflection coefficient and $\theta_1, \dots, \theta_N$ are the phase-shift variables that can be optimized based on \mathbf{g} and \mathbf{h} . With perfect channel knowledge, an achievable SE is⁶ $\log_2(1 + \text{SNR}_{\text{IRS}})$ [14], [40], where

$$\text{SNR}_{\text{IRS}} = |\mathbf{g}^T \mathbf{\Theta} \mathbf{h}|^2 \frac{\mu^2 P_{\text{tx}}}{\sigma^2} = \left| \sum_{n=1}^N |h_n| |g_n| e^{j(\theta_n - \phi_n - \psi_n)} \right|^2 \frac{\mu^2 P_{\text{tx}}}{\sigma^2} \quad (18)$$

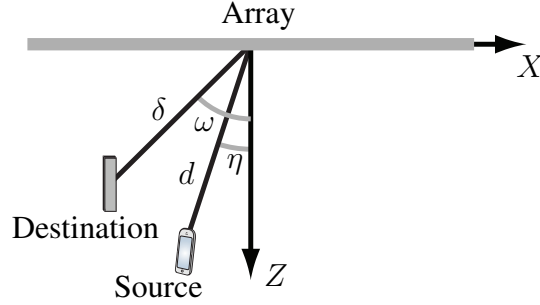
is the SNR at the receiver. We will optimize the phase-shifts in the next section.

⁵An IRS can possibly also adjust the amplitude coefficient between the antennas, but the SNR is maximized when all the amplitude coefficients take the largest possible value, which is here represented by μ . This is why we consider only that value.

⁶Note that this is not the capacity of the IRS-supported channel, but higher SE can be achieved by encoding information into the phase-shift matrix $\mathbf{\Theta}$ [39].



(a) A source at an arbitrary location (x_t, y_t, d) transmits to an planar array located in the XY -plane.



(b) In the analytical parts, the source is at distance d in angle η , while the destination is at distance δ in angle ω .

Fig. 4: Geometric illustration of the setup defined by Assumptions 1 and 2 that is used for analyzing the SNR behavior in the near- and far-fields.

V. POWER SCALING LAWS AND NEAR-FIELD BEHAVIORS

In this section, we investigate the three setups defined in Section IV. Particularly, the power scaling laws, near-field behaviors, and asymptotic SE limits will be analyzed as N increases. New insights into the fundamental properties will be obtained by utilizing the deterministic propagation model derived in Section III. The following assumption is made for all setups.

Assumption 2. *The planar array is centered around the origin in the XY -plane, as illustrated in Fig. 4a. The source is located in the XZ -plane at distance d from the center of the array with angle $\eta \in [-\pi/2, \pi/2]$, as illustrated in Fig. 4b. It sends a signal that has polarization in the Y direction when traveling in the Z direction.*

Under Assumption 2, the source is located at $\mathbf{p}_t = (d \sin(\eta), 0, d \cos(\eta))$ and the n th antenna is centered at $\mathbf{p}_n = (x_n, y_n, 0)$. If we number the antennas from left to right, row by row, according

to Fig. 4a, the coordinates x_n and y_n of the n th receive antenna for $n = 1, \dots, N$ are

$$x_n = -\frac{(\sqrt{N}-1)\sqrt{A}}{2} + \sqrt{A} \bmod(n-1, \sqrt{N}) \quad (19)$$

$$y_n = \frac{(\sqrt{N}-1)\sqrt{A}}{2} - \sqrt{A} \left\lfloor \frac{n-1}{\sqrt{N}} \right\rfloor. \quad (20)$$

A. Massive MIMO

We will now study the mMIMO setup in detail. Following the geometry stated in Assumption 2, we have that $\mathbf{p}_t = (d \sin(\eta), 0, d \cos(\eta))$ and $\mathbf{p}_n = (x_n, y_n, 0)$ where the coordinates x_n and y_n are defined in (19) and (20). By using Lemma 1, the channel $h_n = |h_n|e^{-j\phi_n}$ to the n th receive antenna is obtained as

$$|h_n|^2 = \zeta_{(d \sin(\eta), 0, d \cos(\eta)), (x_n, y_n, 0), \sqrt{A}} \quad (21)$$

and

$$\begin{aligned} \phi_n &= 2\pi \cdot \bmod\left(\frac{\|\mathbf{p}_t - \mathbf{p}_n\|}{\lambda}, 1\right) = 2\pi \cdot \bmod\left(\frac{\sqrt{(x_n - d \sin(\eta))^2 + y_n^2 + d^2 \cos^2(\eta)}}{\lambda}, 1\right) \\ &= 2\pi \cdot \bmod\left(\frac{\sqrt{x_n^2 + y_n^2 + d^2 - 2dx_n \sin(\eta)}}{\lambda}, 1\right). \end{aligned} \quad (22)$$

The following result is then obtained.

Proposition 1. *Under Assumptions 1 and 2, in the mMIMO setup, the SNR with MR combining becomes*

$$\text{SNR}_{\text{mMIMO}} = \xi_{d,\eta,N} \frac{P_{\text{tx}}}{\sigma^2} \quad (23)$$

where the total channel gain $\xi_{d,\eta,N}$ is given by

$$\begin{aligned} \xi_{d,\eta,N} &= \sum_{i=1}^2 \left(\frac{B + (-1)^i \sqrt{B} \tan(\eta)}{6\pi(B+1) \sqrt{2B + \tan^2(\eta) + 1 + 2(-1)^i \sqrt{B} \tan(\eta)}} \right. \\ &\quad \left. + \frac{1}{3\pi} \tan^{-1} \left(\frac{B + (-1)^i \sqrt{B} \tan(\eta)}{\sqrt{2B + \tan^2(\eta) + 1 + 2(-1)^i \sqrt{B} \tan(\eta)}} \right) \right) \end{aligned} \quad (24)$$

with $B = N\pi\beta_{d \cos(\eta)} = \frac{NA}{4d^2 \cos^2(\eta)}$.

Proof: This result follows from Lemma 1 with $\mathbf{p}_t = (d \sin(\eta), 0, d \cos(\eta))$, $\mathbf{p}_n = (0, 0, 0)$, and $a = \sqrt{NA}$. ■

We stress that the channel gain in (24) depends only on the total array area NA (see Remark 1), thus the choice of frequency band only affects how many antennas are needed to achieve that area. Although $\text{SNR}_{\text{mMIMO}}$ in (12) is proportional to the sum of N channel gains and one may be tempted to claim that it grows proportionally to N , the above proposition shows that this is not the case in general. By using Corollary 1, a more compact expression can be obtained when the transmitter is centered in front of the array (i.e., $\eta = 0$).

Corollary 2. *When the transmitter is located in direction $\eta = 0$, the SNR in (23) simplifies to*

$$\text{SNR}_{\text{mMIMO}} = \alpha_{d,N} \frac{P_{\text{tx}}}{\sigma^2} \quad (25)$$

where the total channel gain $\alpha_{d,N}$ is given in (6).

We will now use the general expression in Proposition 1 to study the far-field behavior.

Corollary 3 (Far-field approximation). *If the transmitter is in the far-field of the mMIMO receiver, in the sense that $d \cos(\eta) \gg \sqrt{NA}$, then (25) is well approximated as*

$$\text{SNR}_{\text{mMIMO}} \approx \text{SNR}_{\text{mMIMO}}^{\text{ff}} = N \varsigma_{d,\eta} \frac{P_{\text{tx}}}{\sigma^2} \quad (26)$$

where

$$\varsigma_{d,\eta} = \frac{\beta_{d \cos(\eta)}}{(1 + \tan^2(\eta))^{3/2}} \quad (27)$$

and $\beta_{d \cos(\eta)}$ is given in (2).

Proof: The derivation can be found in Appendix B. ■

We notice that in the far-field, the SNR in (26) is proportional to N , which is consistent with previous work in the mMIMO literature [4], [10], [11]. Hence, when N increases, the system can either benefit from a linearly increasing SNR or reduce P_{tx} as $1/N$ to keep the SNR constant. The latter is the conventional power scaling law for mMIMO, which first appeared in [10], [11]. However, when computing the asymptotic behavior as $N \rightarrow \infty$, these prior works implicitly assumed the transmitter remains in far-field of the array and thus that the SNR goes to infinity as $N \rightarrow \infty$ (or the power can be brought down to zero following the scaling law, while the SNR remains strictly non-zero). This is not physically possible. As N increases, the far-field approximation eventually breaks down and the total channel gain saturates in the near-field, as illustrated in Fig. 2. Unlike [10], [11], the following accurate asymptotic result is provided.

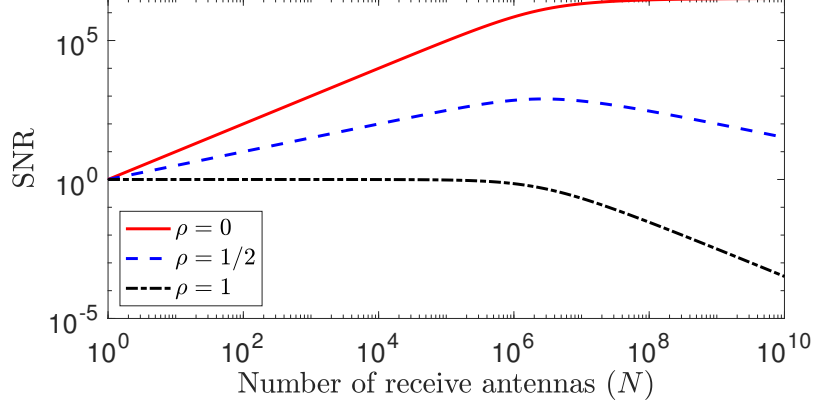


Fig. 5: The SNR value $\text{SNR}_{\text{mMIMO}}$ in (25) when scaling down the transmit power as $P_{\text{tx}} = P/N^\rho$ for $\rho \in \{0, 1/2, 1\}$. The setup in Example 1 is considered with $f = 3 \text{ GHz}$, $\eta = 0$, and P/σ^2 is selected to give $\text{SNR}_{\text{mMIMO}} = 0 \text{ dB}$ for $N = 1$.

Corollary 4 (Asymptotic analysis). *As $N \rightarrow \infty$ with a constant transmit power P_{tx} , the SNR with MR combining satisfies*

$$\text{SNR}_{\text{mMIMO}} \rightarrow \frac{1}{3} \frac{P_{\text{tx}}}{\sigma^2}. \quad (28)$$

If the transmit power is reduced with N as $P_{\text{tx}} = P/N^\rho$ for some constant $P > 0$ and exponent $\rho > 0$, then as $N \rightarrow \infty$

$$\text{SNR}_{\text{mMIMO}} = \xi_{d,\eta,N} \frac{P}{\sigma^2 N^\rho} \rightarrow 0. \quad (29)$$

Proof: The limit in (28) is computed in the same way as the finite limit in (10). Since $P\xi_{d,\eta,N}$ has a finite limit and $1/N^\rho \rightarrow 0$ as $N \rightarrow \infty$, the result in (29) follows directly. ■

This corollary shows that any power scaling for which $P_{\text{tx}} \rightarrow 0$ as $N \rightarrow \infty$ will asymptotically lead to zero SNR. Hence, the asymptotic motivation behind the power scaling laws in the mMIMO literature [10], [11] is misleading. The scaling laws are, nevertheless, useful in many practical situations. To demonstrate this, Fig. 5 shows $\text{SNR}_{\text{mMIMO}}$ in (25) when we scale down the transmit power as $P_{\text{tx}} = P/N^\rho$ for $\rho \in \{0, 1/2, 1\}$, where $\rho = 0$ corresponds to constant power. We consider the setup in Example 1 with $d = 25 \text{ m}$, $\eta = 0$, $f = 3 \text{ GHz}$, and the transmit power is selected so that $P\xi_{d,\eta,N}/\sigma^2 = 0 \text{ dB}$ for $N = 1$. We observe that for $\rho = 0$ the far-field behavior, namely, an SNR that grows linearly with N , approximately holds true for any $N \leq 10^6$, which probably includes all cases of practical interest. If one selects $\rho = 1/2$, the

SNR will instead grow as \sqrt{N} for $N \leq 10^6$. Moreover, for $\rho = 1$, the SNR is approximately constant for $N \leq 10^6$. For larger values of N , the SNR goes to zero whenever $\rho > 0$.

Since this example considers $\eta = 0$, we know from Corollary 2 that $\xi_{d,0,N} = \alpha_{d,N}$. It is the relation between N and d in $\alpha_{d,N}$ that determines when the far-field behavior breaks down. Since these variables enter into $\alpha_{d,N}$ as $N\beta_d = \frac{NA}{4\pi d^2}$, the far-field behavior appear as long as $N/d^2 \leq 10^6/25^2 = 1600$. Hence, even if we would reduce the propagation distance to $d = 2.5$ m, the approximate scaling laws will be accurate for $N \leq 10^4$. In conclusion, the conventional power scaling laws *can be safely applied in practice*, but if we truly want to let $N \rightarrow \infty$, the asymptotically accurate behavior is given by Corollary 4.

B. Massive MIMO Relay

We now turn the attention to the mMIMO relay setup. We assume the destination is equipped with a lossless isotropic antenna located in the XZ -plane at distance δ from the center of the array with angle $\omega \in [-\pi/2, \pi/2]$, as shown in Fig. 4b. This means that it is located at $(\delta \sin(\omega), 0, \delta \cos(\omega))$. According to the geometry stated in Assumption 2, the destination is located at $(\delta \sin(\omega), 0, \delta \cos(\omega))$ and the n th transmit antenna at $(x_n, y_n, 0)$, where x_n and y_n are defined in (19) and (20), respectively. From Lemma 1, it follows that the channel $g_n = |g_n|e^{-j\psi_n}$ from the n th antenna to the destination is given by

$$|g_n|^2 = \zeta_{(\delta \sin(\omega), 0, \delta \cos(\omega)), (x_n, y_n, 0), \sqrt{A}} \quad (30)$$

and

$$\psi_n = 2\pi \cdot \text{mod} \left(\frac{\sqrt{x_n^2 + y_n^2 + \delta^2 - 2\delta x_n \sin(\omega)}}{\lambda}, 1 \right). \quad (31)$$

The following result is then obtained.

Proposition 2. *Suppose the destination is located at distance δ in angle $\omega \in [-\pi/2, \pi/2]$ from the center of the mMIMO relay. Under Assumptions 1 and 2, the SNR with MR precoding becomes*

$$\text{SNR}_{\text{relay}} = \xi_{\delta,\omega,N} \frac{P_{\text{relay}}}{\sigma^2} \quad (32)$$

where the total channel gain $\xi_{\delta,\omega,N}$ is given in (24) and $B = N\pi\beta_{\delta \cos(\omega)} = \frac{NA}{4\delta^2 \cos^2(\omega)}$.

Proof: This result follows from Lemma 1 with $\mathbf{p}_t = (\delta \sin(\omega), 0, \delta \cos(\omega))$, $\mathbf{p}_n = (0, 0, 0)$, and $a = \sqrt{NA}$. ■

By utilizing the results in Proposition 1 and Proposition 2, the end-to-end SE in (15) can be rewritten as

$$\text{SE}_{\text{relay}} = \frac{1}{2} \log_2 \left(1 + \frac{\min(\xi_{d,\eta,N} P_{\text{tx}}, \xi_{\delta,\omega,N} P_{\text{relay}})}{\sigma^2} \right). \quad (33)$$

Note that, when the receiver is centered in front of the array (i.e., $\omega = 0$), we have $\xi_{\delta,0,N} = \alpha_{\delta,N}$.

Just as in the mMIMO setup, the SNR expression takes a simpler approximate form in the far-field, which is now represented by $d \cos(\eta) \gg \sqrt{NA}$ and $\delta \cos(\omega) \gg \sqrt{NA}$. Following a similar approach as in the proof of Corollary 3, we have that

$$\text{SNR}_{\text{relay}} \approx N \varsigma_{\delta,\omega} \frac{P_{\text{relay}}}{\sigma^2} \quad (34)$$

in the far-field, where $\varsigma_{\delta,\omega}$ is defined as in (27). In conjunction with the far-field result in Corollary 3, we obtain the following result in the mMIMO relay setup.

Corollary 5 (Far-field approximation). *If the source and destination are both in the far-field of the mMIMO relay, in the sense that $d \cos(\eta) \gg \sqrt{NA}$ and $\delta \cos(\omega) \gg \sqrt{NA}$, then (33) is well approximated as*

$$\text{SE}_{\text{relay}} \approx \frac{1}{2} \log_2 \left(1 + N \frac{\min(P_{\text{tx}} \varsigma_{d,\eta}, P_{\text{relay}} \varsigma_{\delta,\omega})}{\sigma^2} \right). \quad (35)$$

This corollary shows that the end-to-end SNR grows proportionally to N whenever the far-field approximation is applicable. Hence, one can either keep the transmit powers fixed and achieve an SNR that grows proportionally to N , or reduce the transmit powers P_{tx} and P_{relay} as $1/N$ and achieve the same SNR as with $N = 1$. Since the relay channel is a composition of one uplink and one downlink mMIMO channel, the insights from the last subsection still apply: the far-field approximation and the power scaling law hold in most cases of practical interest. However, in the asymptotic limit as $N \rightarrow \infty$, we have that $\xi_{\delta,\omega,N} \rightarrow \frac{1}{3}$ which is the same asymptotic limit as in the first phase where it holds that $\xi_{d,\eta,N} \rightarrow \frac{1}{3}$. The following corollary shows that the power scaling law breaks down asymptotically.

Corollary 6 (Asymptotic analysis). *As $N \rightarrow \infty$ with constant transmit powers P_{tx} and P_{relay} , the SE with the mMIMO relay satisfies*

$$\text{SE}_{\text{relay}} \rightarrow \frac{1}{2} \log_2 \left(1 + \frac{1}{3} \frac{\min(P_{\text{tx}}, P_{\text{relay}})}{\sigma^2} \right). \quad (36)$$

If the transmit powers are reduced with N as $P_{\text{tx}} = P_1/N^{\rho_1}$ and $P_{\text{relay}} = P_2/N^{\rho_2}$ for some constants $P_1, P_2 > 0$ and exponents $\rho_1, \rho_2 > 0$, then as $N \rightarrow \infty$ it follows that

$$\text{SE}_{\text{relay}} \rightarrow 0. \quad (37)$$

Proof: The proof follows that of Corollary 4 and is therefore omitted. ■

This scaling behavior is essentially the same as the one illustrated in Fig. 5, thus we postpone the numerical comparison with classical mMIMO to Section VI. There are plenty of previous works that study mMIMO relays and the related power scaling laws [19]–[21], often in more general setups (e.g., full-duplex or two-way relaying) than those considered in this paper. Although the power scaling laws developed in those papers are practically relevant, the non-zero asymptotic limits are incorrect since the channel models that are used are asymptotically inaccurate. Since the total channel gain is upper bounded by one (or rather $1/3$ in the considered setup), any power scaling law that leads to zero transmit power as $N \rightarrow \infty$ must also have a zero-valued asymptotic SE. Corollary 6 demonstrates this in a simple decode-and-forward relay setup but the result naturally extends to more complicated setups.

C. Intelligent Reflecting Surface

We begin by observing that the SNR is maximized in (18) when all the terms in the summation has the same phase [14], [40]. This is achieved, for example, by selecting $\theta_n = \phi_n + \psi_n$ for $n = 1, \dots, N$. In doing this, (18) becomes

$$\text{SNR}_{\text{IRS}} = \frac{\mu^2 P_{\text{tx}}}{\sigma^2} \left(\sum_{n=1}^N |h_n| |g_n| \right)^2. \quad (38)$$

We can compute this expression exactly using (21) and (30). We can also obtain the following simple and tight upper bound that does not involve any summations.

Proposition 3. *The SNR in (38) with optimal phase-shifts can be upper bounded as*

$$\begin{aligned} \text{SNR}_{\text{IRS}} &\leq \text{SNR}_{\text{IRS}}^{\text{upper}} = \left(\sum_{n=1}^N |h_n|^2 \right) \left(\sum_{n=1}^N |g_n|^2 \right) \frac{\mu^2 P_{\text{tx}}}{\sigma^2} = \xi_{d,\eta,N} \xi_{\delta,\omega,N} \frac{\mu^2 P_{\text{tx}}}{\sigma^2} \\ &= \mu^2 \xi_{\delta,\omega,N} \text{SNR}_{\text{mMIMO}} \end{aligned} \quad (39)$$

with $\text{SNR}_{\text{mMIMO}}$ given in (23). The equality holds if and only if the vectors $[|h_1|, \dots, |h_N|]^T$ and $[|g_1|, \dots, |g_N|]^T$ are parallel.

Proof: The inequality is a direct application of Hölder's inequality, followed by computing the total channel gains of the two links using Proposition 1. ■

Interestingly, the upper bound in (39) is the product of the SNR in the mMIMO setup and the terms μ^2 and $\xi_{\delta,\omega,N}$, which are the fraction of power that is reflected by the IRS and the total

channel gain from the IRS to the destination, respectively. None of the latter two terms can be larger than one; in particular, Section II described that the value of $\xi_{\delta,\omega,N}$ must be below one (or rather $1/3$) due to the law of energy conservation. Therefore, Proposition 3 implicitly states that the IRS setup cannot achieve a higher SNR than the corresponding mMIMO setup, if the array sizes are equal. One way to interpret this result is that the IRS acts as an uplink mMIMO receiver that uses the receive combining $\mathbf{v} = \Theta^T \mathbf{g}$, which has a different directivity than the channel \mathbf{h} , except when $[|h_1|, \dots, |h_N|]^T$ and $[|g_1|, \dots, |g_N|]^T$ are parallel vectors. In any case, it also incurs an additional SNR loss given by

$$\|\mathbf{v}\|^2 = \|\Theta^T \mathbf{g}\|^2 = \mu^2 \|\mathbf{g}\|^2 = \mu^2 \xi_{\delta,\omega,N} < 1. \quad (40)$$

Similar conclusions hold when the IRS is compared to the mMIMO relay. To see this, assume for simplicity that the transmit power is the same in the two phases (i.e., $P_{\text{relay}} = P_{\text{tx}}$). In this case, we may equivalently rewrite (39) as

$$\text{SNR}_{\text{IRS}}^{\text{upper}} = \mu^2 \xi_{d,\eta,N} \text{SNR}_{\text{relay}} \quad (41)$$

which can never be higher than $\text{SNR}_{\text{relay}}$, based on the same arguments as above. Since the end-to-end SNR of the mMIMO relay channel is the minimum of the SNRs in the two phases, i.e., $\min(\text{SNR}_{\text{relay}}, \text{SNR}_{\text{mMIMO}})$, and both are higher than $\text{SNR}_{\text{IRS}}^{\text{upper}}$, we can conclude that the IRS can never achieve a higher SNR than the corresponding mMIMO relay setup with a matching array size and transmit power. However, the relay suffers from the $1/2$ pre-log factor in (15), which can potentially make the IRS more spectrally efficient, even if the SNR is lower. To investigate this further, assume that $\text{SNR}_{\text{relay}} > \text{SNR}_{\text{mMIMO}}$ so that (15) becomes

$$\text{SE}_{\text{relay}} = \frac{1}{2} \log_2 (1 + \text{SNR}_{\text{mMIMO}}). \quad (42)$$

From (39), the SE with the IRS is upper bounded by $\log_2(1 + \mu^2 \xi_{\delta,\omega,N} \text{SNR}_{\text{mMIMO}})$, which is lower than (42) when

$$\mu^2 \xi_{\delta,\omega,N} < \frac{\sqrt{1 + \text{SNR}_{\text{mMIMO}}} - 1}{\text{SNR}_{\text{mMIMO}}}. \quad (43)$$

This condition may not be satisfied when $\text{SNR}_{\text{mMIMO}}$ is large. Hence, there are high-SNR cases when the IRS setup outperforms the mMIMO relay. This observation is in line with previous results in [17], [40].

We will now study the power scaling law. Recall from (38) that the SNR is proportional to the square of a sum with N terms. Intuitively, the SNR may then grow quadratically with N . That behavior can in fact be observed in the far-field.

Corollary 7 (Far-field approximation). *If both the source and destination are in the far-field of the IRS, in the sense that $d \cos(\eta) \gg \sqrt{NA}$ and $\delta \cos(\omega) \gg \sqrt{NA}$, the SNR in (38) can be approximated as*

$$\text{SNR}_{\text{IRS}} \approx \text{SNR}_{\text{IRS}}^{\text{ff}} = N^2 \varsigma_{d,\eta} \varsigma_{\delta,\omega} \frac{\mu^2 P_{\text{tx}}}{\sigma^2}. \quad (44)$$

Proof: This result is proved in the same way as Corollary 3 and Corollary 5. ■

The quadratic scaling with N in (35) has been recognized in several recent works [14], [18], [22], but without explaining that it only holds under a far-field approximation. Moreover, those papers noticed that SNR growth is faster than the linear scaling with N observed for mMIMO receiver in (26) and for the mMIMO relay in (35). Although that implies that an IRS benefits more from increasing the array size, it does not mean that it will achieve a higher SNR when N is large. Indeed, we already know from Proposition 3 and the subsequent discussion that this cannot happen in neither the far-field nor the near-field.

The right way of interpreting the N^2 scaling can be seen by factorizing the far-field SNR in (44) into two factors:

$$\text{SNR}_{\text{IRS}}^{\text{ff}} = \underbrace{\mu^2 N \varsigma_{\delta,\omega}}_{\leq 1, \text{ Fraction of reflected power reaching destination}} \times \underbrace{N \varsigma_{d,\eta} \frac{P_{\text{tx}}}{\sigma^2}}_{=\text{SNR}_{\text{mMIMO}}^{\text{ff}}}. \quad (45)$$

The first factor contains one N -term and describes the fraction of power received at the IRS that also reaches the destination. Since this term is fundamentally upper bounded by one, this N -term describes a drawback rather than a benefit of using IRS (it is the fraction of power that is *not* lost). The second factor in (45) equals the far-field mMIMO SNR in (26) and its N -term represents the power/array gain that is achieved when having a large array.

To demonstrate these properties, Fig. 6 shows the total channel gains obtained by the mMIMO receiver and the IRS setup for a varying number of antennas/elements N . We consider the setup in Example 1 with $d = 25$ m, $\eta = \pi/6$, $\delta = 2.5$ m, $\omega = -\pi/6$, $f = 3$ GHz, and $\mu = 1$ (i.e., no reflection loss). Notice that in the IRS setup, the destination is in the vicinity of the IRS. The figure shows that the total channel gain grows as N^2 with the IRS and as N with the mMIMO receiver, which is consistent with the respective far-field approximations. Nevertheless, mMIMO provides a much larger channel gain for most values of N , which is consistent with Proposition 3. The advantage remains asymptotically. The reason is that each element of the IRS acts as a scatterer, so that the IRS setup can be viewed as a relay that forwards the signal to the

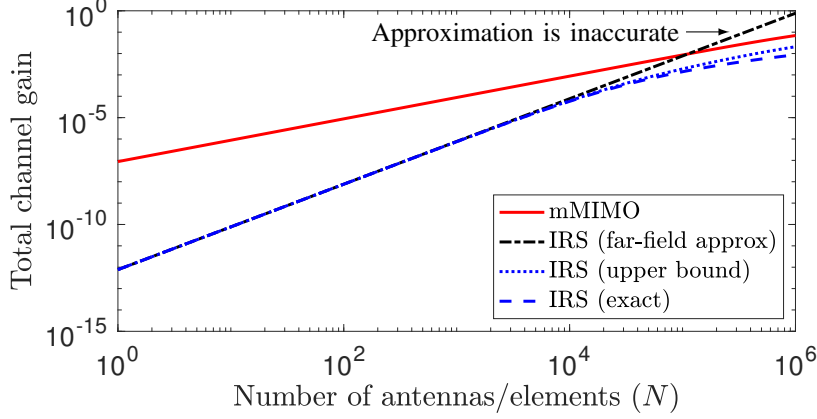


Fig. 6: The total channel gain obtained with the mMIMO receiver and with the IRS setup, for different number of antennas/elements N . The setup in Example 1 is considered with $d = 25$ m, $\eta = \pi/6$, $\delta = 2.5$ m, $\omega = -\pi/6$, $f = 3$ GHz, and $\mu = 1$.

destination without amplifying it [40]. Even if the destination is close to the IRS, the far-field approximation in (44) is accurate until the IRS has roughly 10^4 elements. The upper bound in (39) follows the exact curve closely, even for $N > 10^4$, which is why we called it a tight bound.

Remark 3. *The upper bound in Proposition 3 contains the product of the total channel gain $\xi_{d,\eta,N}$ between the source and IRS and the total channel gain $\xi_{\delta,\omega,N}$ between the IRS and the destination. This is the same structure as for the far-field SNR in (44), which has previously been analyzed in a series of previous works (e.g., [23], [26], [27], [38]). However, the near-field behavior has not been analytically studied with the same rigor. The IRS was modeled as a specular reflector (i.e., an ideal mirror) in [18], [23]–[25] and the channel gain in the near-field can then be made proportional to $1/(d + \delta)^2$ [25]. This expression is different from the upper bound in Proposition 3, where there are no terms that depend on both d and δ . The following conclusion can be made: If one can operate an IRS to get a channel gain of the kind in [18], [23]–[25], the SNR is likely not maximized. We return to this matter in Section VII.*

We conclude this section by using the upper bound in Proposition 3 to study the asymptotic behavior of an IRS, particularly in the near-field.

Corollary 8 (Asymptotic analysis). *As $N \rightarrow \infty$ with constant transmit power P_{tx} , the SNR in the IRS setup is asymptotically upper bounded since*

$$\text{SNR}_{\text{IRS}}^{\text{upper}} \rightarrow \frac{1}{9} \frac{\mu^2 P_{\text{tx}}}{\sigma^2}. \quad (46)$$

If the transmit power is reduced with N as $P_{\text{tx}} = P/N^\rho$ for some constant $P > 0$ and exponent $\rho > 0$, then as $N \rightarrow \infty$ it follows that

$$\text{SNR}_{\text{IRS}} = \left(\sum_{n=1}^N |h_n| |g_n| \right)^2 \frac{\mu^2 P}{N^\rho \sigma^2} \rightarrow 0. \quad (47)$$

Proof: The upper bound follows from the fact that $\xi_{d,\eta,N}, \xi_{\delta,\omega,N} \rightarrow 1/3$ as $N \rightarrow \infty$, which was also utilized in Corollary 4. Since the channel gain is upper bounded, the SNR goes to zero if P_{tx} goes asymptotically to zero. ■

This corollary shows, once again, that the asymptotic SE limit of any conventional power scaling law is zero. Nevertheless, we can expect the SNR in the IRS setup to grow as N^2 for most practical array sizes. In agreement with Proposition 3, Corollary 8 also shows that an IRS setup can never reach the same SNR as the mMIMO receiver for any common value of N . The difference remains even as $N \rightarrow \infty$.

VI. HOW MANY ELEMENTS ARE NEEDED FOR THE IRS SETUP TO BE COMPETITIVE?

When looking for suitable use cases for the IRS technology, one needs to ask the question: How *large* must the IRS be to achieve the same performance as with an active mMIMO receiver or an mMIMO relay? To answer this question, we now let N_{mMIMO} , N_{relay} , and N_{IRS} , denote the number of elements of the mMIMO receiver, the mMIMO relay, and the IRS, respectively. We can then determine how many elements are needed in the IRS to achieve the same or higher SE than with the competing technologies.

Corollary 9. *When operating in the far-field, the IRS case provides higher SE than the mMIMO receiver if*

$$N_{\text{IRS}} \geq \sqrt{\frac{N_{\text{mMIMO}}}{\mu^2 \zeta_{\delta,\omega}}}. \quad (48)$$

Similarly, the IRS case provides higher SE than the mMIMO relay if

$$N_{\text{IRS}} \geq \frac{\sigma^2}{\mu^2 P_{\text{tx}} \zeta_{d,\eta} \zeta_{\delta,\omega}} \sqrt{1 + N_{\text{relay}} \frac{\min(P_{\text{tx}} \zeta_{d,\eta}, P_{\text{relay}} \zeta_{\delta,\omega})}{\sigma^2}}. \quad (49)$$

Proof: This follows from comparing the expressions in Corollaries 3, 5, and 7. ■

By inserting values into the expressions in Corollary 9, Fig. 7 shows how many antennas are needed to achieve a particular SE in each of the three setups. The same simulation parameters as in Fig. 6 are considered. The first observation is that the IRS needs more than 100 elements

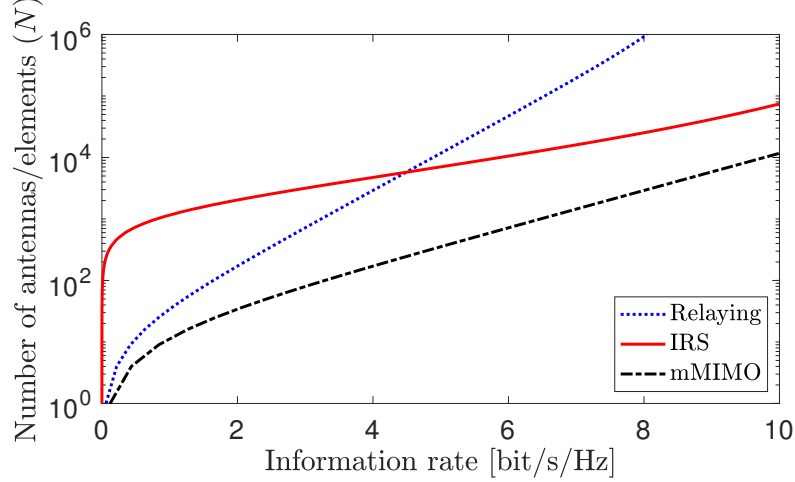


Fig. 7: The number of elements/antennas needed to achieve a given information rate in the different setups. The parameters in Example 1 are considered with $d = 25$ m, $\eta = \pi/6$, $\delta = 2.5$ m, $\omega = -\pi/6$, $f = 3$ GHz, and $\mu = 1$.

before it provides an SE that is clearly above zero. After that, the number of elements grows more gracefully with the SE than for the relay and mMIMO setups, since the SNR grows as N^2 . However, it is only for SEs greater than 4.5 bit/s/Hz that $N_{\text{IRS}} < N_{\text{relay}}$. The IRS must always be larger than the mMIMO array to deliver the same SE. For example, $N_{\text{mMIMO}} = 100$ delivers 3.3 bit/s/Hz, while $N_{\text{IRS}} \approx 3500$ is needed to achieve the same SE. The gap reduces asymptotically but will not vanish, as proved in the previous section.

VII. GEOMETRIC INTERPRETATION OF OPTIMIZED IRS

Some recent works model an IRS as a specular reflector or an “anomalous mirror” (i.e., a mirror with an unusual reflection angle) [18], [23]–[25], which basically means that the IRS reflects the incoming signal towards the destination as a flat and perfectly rotated mirror would do. Under these conditions, the total channel gain of the IRS setup would converge to

$$\zeta_{d,\delta}^{\text{mirror}} = \frac{A}{4\pi(d + \delta)^2} \quad (50)$$

when the array is sufficiently large and the near-field is considered. This asymptotic formula can be motivated by geometrical physics if one considers an equivalent setup where the destination is behind the mirror and the total propagation distance is $d + \delta$. Interestingly, the limit in (50) differs from the asymptotic upper bound in Corollary 8. Moreover, as already pointed out in Remark 3, the two distances d and δ appear in (50) in a joint factor $(d + \delta)^2$ and not within separate multiplicative factors as in Proposition 3.

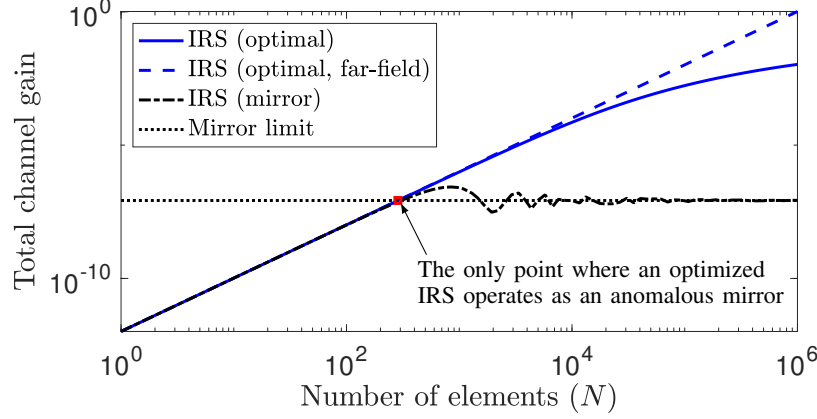


Fig. 8: The total channel gain obtained with the IRS-aided communication using either optimal phases or mirror-mimicking phases, for different number of elements N . The setup in Example 1 is considered with $f = 3$ GHz, $d = 25$ m, $\eta = 0$, $\delta = 2.5$ m, $\omega = 0$, and $\mu = 1$.

The reason for the different expressions is that an optimized IRS *does not operate as a mirror*. If a plane wave is impinging on a mirror, its specular reflection is also a plane wave. In contrast, if a plane wave is impinging on an IRS, each element will scatter a piece of the wave with a particular phase-shift. By optimizing the phase-shifts so that the N scattered waves add constructively at the destination, the IRS effectively operates as a lens that focuses the incoming wave at the point of destination.

Fig. 8 demonstrates this in a setup where both the source and destination are centered in front of the array (i.e., $d = 25$ m, $\eta = 0$, $\delta = 2.5$ m, $\omega = 0$), following Example 1 with $f = 3$ GHz and $\mu = 1$. In this case, a mirror-mimicking IRS has $\theta_n = 0$ for all n and the corresponding total channel gain can be computed using (18) as $|\sum_{n=1}^N |h_n| |g_n| e^{-j(\phi_n + \psi_n)}|^2$. Fig. 8 also reports the total channel gain $(\sum_{n=1}^N |h_n| |g_n|)^2$ of an optimized IRS with $\theta_n = \phi_n + \psi_n$. There is no noticeable difference in the figure for small IRSs because when the source and destination are in the far-field, focusing the incoming (approximately) plane wave on a far-away point is approximately the same as mimicking a mirror that reflects the signal in the angular direction of that point. However, at around $N = 200$, the channel gain of the mirror-mimicking IRS starts to converge to (50), while the channel gain of the optimized IRS continues to increase. At $N = 10^4$, the optimized IRS has a 100 times better channel gain than the mirror limit in (50). We conclude that the SNR achieved by an *optimized IRS* can generally not be described using the mirror limit; particularly not in the near-field since the far-field approximation is accurate far beyond the point

where optimized SNR surpasses the mirror limit. This conclusion is consistent with the results in [26]. However, one can certainly use the mirror analogy to identify the approximately optimal phase-shifts when operating in the far-field [38].

By setting the far-field approximation in (44), for an optimized IRS, equal to the mirror limit in (50), we obtain that

$$NA = \left(\frac{1}{d} + \frac{1}{\delta} \right)^{-1} \lambda \quad (51)$$

is the largest array area that a mirror-mimicking IRS can make use of in this example.⁷ This point is indicated by a square in Fig. 8. If the IRS is larger, the remaining area is essentially wasted on scattering signals in other directions. In other words, if one uses (50) as a proxy for the channel gain of an optimized IRS (e.g., as done in [18], [24]), then the results only hold when the IRS has exactly the area in (51) and the source/destination are centered in front of it. If we change δ or λ , the curves in Fig. 8 will be shifted in different directions, but the quantitative conclusions remain the same. In summary, the correct geometric interpretation of an optimized IRS is a reconfigurable lens that can focus any incoming wave onto the point of destination.

VIII. CONCLUSIONS

The limit of large number of antennas has been studied in the MIMO literature for decades. In this paper, we have noticed that previous asymptotic analyses have used channel models that are only accurate in the far-field, while the asymptotic limit can only be approached when operating the near-field. Hence, the asymptotic SE behaviors and power scaling laws in the existing literature can be misleading. To address this issue, we have derived a physically accurate channel gain expression for planar arrays, taking both polarization and near-field conditions (such as varying effective antenna areas) into account. We have used this model to revisit the power scaling laws and asymptotic limits in three MIMO setups: mMIMO, mMIMO relays, and IRS.

The main observations are as follows. The total channel gains in the two mMIMO setups grow as N in the far-field, where N is the number of antennas/elements, while it grows as N^2 in the IRS setup. Numerical results showed that these behaviors are accurate even when the arrays have thousands of elements/antennas, thus the classical scaling results are accurate in most practical deployments. However, the growth rate eventually tapers off when entering the near-field, and the channel gain converges to $1/3$ as $N \rightarrow \infty$ in the mMIMO setups, and is upper bounded

⁷The expression is generalized in [26, Eq. (35)] to cases where the source and destination are located in different directions.

by $1/9$ in the IRS setup. Consequently, any power scaling law that lets the transmit power go asymptotically to zero will also lead to zero asymptotic SE.

The IRS will provably always achieve a lower SNR than the two mMIMO setups for any common value of N , despite the faster growth rate observed in the far-field. The reason is that one of the N -terms in the SNR accounts for the fraction of power that is lost in the IRS's reflection, thus it represents a drawback rather than a benefit. However, if the IRS has a larger array size than in the mMIMO setups, it can achieve a higher SNR. Needless to say, the cost per element is lower with an IRS than in mMIMO, thus the IRS can still be of practical interest.

By using the analytical expressions, we have proved that the SNR of an *optimized* IRS contains the product of the channel gains from the source to the IRS and from the IRS to the destination, in both the near-field and the far-field. Previous works have interpreted the IRS as an anomalous mirror (specular reflector) that can control the angular direction of the “reflected” signal, but we stress that an optimized IRS is a reconfigurable lens since it can also focus the signal on a point in the near-field. One can use the mirror analogy in the far-field to identify appropriate phase shifts, but the optimal SNR does not match the “sum-of-distances” expression appearing for an ideal mirror. In the near-field, the IRS can achieve SNRs far beyond what that mirror limit.

APPENDIX A - PROOF OF LEMMA 1

The proof of this lemma will make use of the following primitive functions:

$$\int \frac{\partial x}{(x^2 + a)^{3/2}} = \frac{x}{a\sqrt{x^2 + a}} + C \quad (52)$$

$$\int \frac{\partial x}{(x^2 + a)^{5/2}} = \frac{x}{3a(x^2 + a)^{3/2}} + \frac{2x}{3a^2\sqrt{x^2 + a}} + C \quad (53)$$

$$\int \frac{\partial x}{(x^2 + a)\sqrt{x^2 + a + b}} = \frac{1}{\sqrt{ab}} \tan^{-1} \left(\frac{\sqrt{b}x}{\sqrt{a}\sqrt{x^2 + a + b}} \right) + C \quad (54)$$

where a, b are arbitrary scalars and C is an arbitrary constant.

The channel gain $\zeta_{\mathbf{p}_t, \mathbf{p}_n}$ with a lossless isotropic transmit antenna and polarization in the Y direction (when the signal travels in the Z direction) can be computed as [33, Eq. (16)] by exchanging the X and Y dimensions:

$$\begin{aligned} & \underbrace{\iint_{\text{Antenna area}} \frac{d}{\sqrt{(r_x - x_t)^2 + (r_y - y_t)^2 + d^2}}}_{\text{Reduction in effective area from directivity}} \underbrace{\frac{(r_x - x_t)^2 + d^2}{(r_x - x_t)^2 + (r_y - y_t)^2 + d^2}}_{\text{Polarization loss factor}} \underbrace{\frac{\partial r_x \partial r_y}{4\pi((r_x - x_t)^2 + (r_y - y_t)^2 + d^2)}}_{\text{Free-space pathloss}} \\ &= \frac{1}{4\pi} \int_{x_n - a/2}^{x_n + a/2} \int_{y_n - a/2}^{y_n + a/2} \frac{d((r_x - x_t)^2 + d^2) \partial r_x \partial r_y}{((r_x - x_t)^2 + (r_y - y_t)^2 + d^2)^{5/2}} \end{aligned} \quad (55)$$

where r_x, r_y are integration variables representing the location of the receive antenna. The contributions of the three fundamental properties when operating in the near-field of the array (i.e., the distance to the elements, the effective antenna areas, the loss from polarization) are clearly explicated. Next, we make the change of variables $\chi = r_x - x_t$ and $v = r_y - y_t$, so that (55) becomes

$$\frac{1}{4\pi} \int_{x_n-a/2-x_t}^{x_n+a/2-x_t} \int_{y_n-a/2-y_t}^{y_n+a/2-y_t} \frac{d(\chi^2 + d^2) \partial v \partial \chi}{(\chi^2 + v^2 + d^2)^{5/2}} =$$

$$\frac{1}{4\pi} \int_{x_n-a/2-x_t}^{x_n+a/2-x_t} \left[\frac{vd}{3(\chi^2 + v^2 + d^2)^{3/2}} + \frac{2vd}{3(\chi^2 + d^2)\sqrt{\chi^2 + v^2 + d^2}} \right]_{y_n-a/2-y_t}^{y_n+a/2-y_t} \partial \chi = \quad (56)$$

$$\frac{1}{4\pi} \left(\sum_{y \in \mathcal{Y}} \int_{x_n-a/2-x_t}^{x_n+a/2-x_t} \frac{yd}{3(\chi^2 + y^2 + d^2)^{3/2}} \partial \chi + \sum_{y \in \mathcal{Y}} \int_{x_n-a/2-x_t}^{x_n+a/2-x_t} \frac{2yd}{3(\chi^2 + d^2)\sqrt{\chi^2 + y^2 + d^2}} \partial \chi \right) \quad (57)$$

by utilizing (53). The first integral in (57) can now be computed using (52) as

$$\int_{x_n-a/2-x_t}^{x_n+a/2-x_t} \frac{yd}{3(\chi^2 + y^2 + d^2)^{3/2}} \partial \chi = \sum_{x \in \mathcal{X}} \frac{xyd}{(y^2 + d^2)\sqrt{x^2 + y^2 + d^2}}. \quad (58)$$

Moreover, the second integral in (57) can be computed using (54) as

$$\int_{x_n-a/2-x_t}^{x_n+a/2-x_t} \frac{2yd}{3(\chi^2 + d^2)\sqrt{\chi^2 + y^2 + d^2}} \partial \chi = \sum_{x \in \mathcal{X}} \frac{2}{3} \tan^{-1} \left(\frac{xy}{d\sqrt{x^2 + y^2 + d^2}} \right). \quad (59)$$

Substituting (58) into (56) and (59) into (57) yield the final result in (4), after dividing the numerators and denominators by d .

APPENDIX B - PROOF OF COROLLARY 3

When $d \cos(\eta) \gg \sqrt{NA}$, it follows that $B + 1 \approx 1$ and $2B + 1 \approx 1$. We can then utilize that $\tan^{-1}(x) \approx x$ for $x \approx 0$ to approximate (24) as

$$\xi_{d,\eta,N} \approx \sum_{i=1}^2 \frac{B + (-1)^i \sqrt{B} \tan(\eta)}{2\pi \sqrt{\tan^2(\eta) + 1 + 2(-1)^i \sqrt{B} \tan(\eta)}}. \quad (60)$$

Furthermore, we can utilize that $\sqrt{1+x} \approx 1 + x/2$ for $x \approx 0$ to approximate the denominator of (60) and obtain

$$\xi_{d,\eta,N} \approx \sum_{i=1}^2 \frac{B + (-1)^i \sqrt{B} \tan(\eta)}{2\pi \sqrt{1 + \tan^2(\eta)} \left(1 + \frac{(-1)^i \sqrt{B} \tan(\eta)}{1 + \tan^2(\eta)} \right)} = \frac{2B - \frac{2B \tan^2(\eta)}{1 + \tan^2(\eta)}}{2\pi \sqrt{1 + \tan^2(\eta)} \left(1 + \frac{\sqrt{B} \tan(\eta)}{1 + \tan^2(\eta)} \right) \left(1 - \frac{\sqrt{B} \tan(\eta)}{1 + \tan^2(\eta)} \right)}$$

$$\approx \frac{B}{\pi(1 + \tan^2(\eta))^{3/2}} = N\beta_{d,\eta} \quad (61)$$

where we first simplified the expression by writing the two fractions as a single fraction and then utilized that $1 - \frac{(-1)^i \sqrt{B} \tan(\eta)}{1 + \tan^2(\eta)} \approx 1$.

REFERENCES

- [1] E. Björnson and L. Sanguinetti, “Demystifying the power scaling law of intelligent reflecting surfaces and metasurfaces,” in *Proc. IEEE International Workshop on Computational Advances in Multi-Sensor Adaptive Processing (CAMSAP)*, 2019.
- [2] S. Parkvall, E. Dahlman, A. Furuskär, and M. Frenne, “NR: The new 5G radio access technology,” *IEEE Communications Standards Magazine*, vol. 1, no. 4, pp. 24–30, 2017.
- [3] T. L. Marzetta, “Noncooperative cellular wireless with unlimited numbers of base station antennas,” *IEEE Trans. Wireless Commun.*, vol. 9, no. 11, pp. 3590–3600, 2010.
- [4] E. Björnson, J. Hoydis, and L. Sanguinetti, “Massive MIMO networks: Spectral, energy, and hardware efficiency,” *Foundations and Trends® in Signal Processing*, vol. 11, no. 3-4, pp. 154–655, 2017.
- [5] L. Sanguinetti, E. Björnson, and J. Hoydis, “Towards massive MIMO 2.0: Understanding spatial correlation, interference suppression, and pilot contamination,” *IEEE Trans. Commun.*, vol. 68, no. 1, pp. 232–257, 2020.
- [6] E. Björnson, L. Sanguinetti, H. Wymeersch, J. Hoydis, and T. L. Marzetta, “Massive MIMO is a reality—What is next? Five promising research directions for antenna arrays,” *Digital Signal Processing*, vol. 94, pp. 3–20, Nov. 2019.
- [7] S. Hu, F. Rusek, and O. Edfors, “Beyond massive MIMO: The potential of data transmission with large intelligent surfaces,” *IEEE Trans. Signal Process.*, vol. 66, no. 10, pp. 2746–2758, 2018.
- [8] A. Amiri, M. Angjelichinoski, E. de Carvalho, and R. W. Heath, “Extremely large aperture massive MIMO: Low complexity receiver architectures,” in *IEEE Global Communications Conference Workshops (GLOBECOM Workshops)*, 2018.
- [9] A. Pizzo, T. L. Marzetta, and L. Sanguinetti, “Spatially-stationary model for holographic MIMO small-scale fading,” *CoRR*, vol. abs/1911.04853, 2019.
- [10] H. Q. Ngo, E. G. Larsson, and T. L. Marzetta, “Energy and spectral efficiency of very large multiuser MIMO systems,” *IEEE Trans. Commun.*, vol. 61, no. 4, pp. 1436–1449, 2013.
- [11] J. Hoydis, S. ten Brink, and M. Debbah, “Massive MIMO in the UL/DL of cellular networks: How many antennas do we need?” *IEEE J. Sel. Areas Commun.*, vol. 31, no. 2, pp. 160–171, 2013.
- [12] L. Liang, M. Qi, J. Yang, X. Shen, J. Zhai, W. Xu, B. Jin, W. Liu, Y. Feng, C. Zhang, H. Lu, H.-T. Chen, L. Kang, W. Xu, J. Chen, T. J. Cui, P. Wu, and S. Liu, “Anomalous terahertz reflection and scattering by flexible and conformal coding metamaterials,” *Advanced Optical Materials*, vol. 3, no. 10, pp. 1374–1380, 2015.
- [13] A. M. H. Wong and G. V. Eleftheriades, “Perfect anomalous reflection with a bipartite huygens’ metasurface,” *Phys. Rev. X*, vol. 8, p. 011036, 2018.
- [14] Q. Wu and R. Zhang, “Intelligent reflecting surface enhanced wireless network via joint active and passive beamforming,” *IEEE Trans. Wireless Commun.*, vol. 18, no. 11, pp. 5394–5409, Nov 2019.
- [15] C. Liaskos, S. Nie, A. Tsioliaridou, A. Pitsillides, S. Ioannidis, and I. Akyildiz, “A new wireless communication paradigm through software-controlled metasurfaces,” *IEEE Commun. Mag.*, vol. 56, no. 9, pp. 162–169, 2018.
- [16] M. D. Renzo, M. Debbah, D.-T. Phan-Huy, A. Zappone, M.-S. Alouini, C. Yuen, V. Sciancalepore, G. C. Alexandropoulos, J. Hoydis, H. Gacanin, J. de Rosny, A. Bounceu, G. Lerosey, and M. Fink, “Smart radio environments empowered by reconfigurable AI meta-surfaces: an idea whose time has come,” *EURASIP Journal on Wireless Communications and Networking*, vol. 2019:129, 2019.
- [17] C. Huang, A. Zappone, G. C. Alexandropoulos, M. Debbah, and C. Yuen, “Reconfigurable intelligent surfaces for energy efficiency in wireless communication,” *IEEE Trans. Wireless Commun.*, vol. 18, no. 8, pp. 4157–4170, 2019.
- [18] E. Basar, M. Di Renzo, J. De Rosny, M. Debbah, M. Alouini, and R. Zhang, “Wireless communications through reconfigurable intelligent surfaces,” *IEEE Access*, vol. 7, pp. 116 753–116 773, 2019.

- [19] H. Q. Ngo, H. A. Suraweera, M. Matthaiou, and E. G. Larsson, "Multipair full-duplex relaying with massive arrays and linear processing," *IEEE J. Sel. Areas Commun.*, vol. 32, no. 9, pp. 1721–1737, Sep. 2014.
- [20] X. Yang, X. Liang, X. Zhang, S. Jin, and T. Song, "Power scaling laws for massive MIMO relay systems with linear transceivers," in *IEEE Global Conference on Signal and Information Processing (GlobalSIP)*, Dec 2015, pp. 38–42.
- [21] C. Kong, C. Zhong, M. Matthaiou, E. Björnson, and Z. Zhang, "Multipair two-way half-duplex DF relaying with massive arrays and imperfect CSI," *IEEE Trans. Wireless Commun.*, vol. 17, no. 5, pp. 3269–3283, May 2018.
- [22] Q. Wu and R. Zhang, "Towards smart and reconfigurable environment: Intelligent reflecting surface aided wireless network," *IEEE Commun. Mag.*, vol. 58, no. 1, pp. 106–112, 2020.
- [23] W. Tang, M. Z. Chen, X. Chen, J. Y. Dai, Y. Han, M. D. Renzo, Y. Zeng, S. Jin, Q. Cheng, and T. J. Cui, "Wireless communications with reconfigurable intelligent surface: Path loss modeling and experimental measurement," *CoRR*, vol. abs/1911.05326, 2019.
- [24] I. Yildirim, A. Uyrus, E. Basar, and I. F. Akyildiz, "Propagation modeling and analysis of reconfigurable intelligent surfaces for indoor and outdoor applications in 6G wireless systems," *CoRR*, vol. abs/1912.07350, 2019.
- [25] M. D. Renzo, F. H. Danufane, X. Xi, J. de Rosny, and S. Tretyakov, "Analytical modeling of the path-loss for reconfigurable intelligent surfaces—anomalous mirror or scatterer?" *CoRR*, vol. abs/2001.10862, 2020.
- [26] S. W. Ellingson, "Path loss in reconfigurable intelligent surface-enabled channels," *CoRR*, vol. abs/1912.06759, 2019.
- [27] J. Garcia, A. Sibille, and M. Kamoun, "Reconfigurable intelligent surfaces: Bridging the gap between scattering and reflection," *CoRR*, vol. abs/1912.05344, 2019.
- [28] H. T. Friis, "A note on a simple transmission formula," *IRE*, vol. 34, no. 5, pp. 254–256, 1946.
- [29] J. Jose, A. Ashikhmin, T. L. Marzetta, and S. Vishwanath, "Pilot contamination and precoding in multi-cell TDD systems," *IEEE Trans. Commun.*, vol. 10, no. 8, pp. 2640–2651, 2011.
- [30] H. Yin, D. Gesbert, M. Filippou, and Y. Liu, "A coordinated approach to channel estimation in large-scale multiple-antenna systems," *IEEE J. Sel. Areas Commun.*, vol. 31, no. 2, pp. 264–273, 2013.
- [31] R. Müller, L. Cottatellucci, and M. Vehkaperä, "Blind pilot decontamination," *IEEE J. Sel. Topics Signal Process.*, vol. 8, no. 5, pp. 773–786, 2014.
- [32] E. Björnson, J. Hoydis, and L. Sanguinetti, "Massive MIMO has unlimited capacity," *IEEE Trans. Wireless Commun.*, vol. 17, no. 1, pp. 574–590, Jan. 2018.
- [33] D. Dardari, "Communication with large intelligent surfaces: Fundamental limits and models," *CoRR*, vol. abs/1912.01719, 2019.
- [34] E. Telatar, "Capacity of multi-antenna Gaussian channels," *European Trans. Telecom.*, vol. 10, no. 6, pp. 585–595, 1999.
- [35] J. N. Laneman, D. N. C. Tse, and G. W. Wornell, "Cooperative diversity in wireless networks: Efficient protocols and outage behavior," *IEEE Trans. Inf. Theory*, vol. 50, no. 12, pp. 3062–3080, 2004.
- [36] G. Farhadi and N. C. Beaulieu, "On the ergodic capacity of multi-hop wireless relaying systems," *IEEE Trans. Wireless Commun.*, vol. 8, no. 5, pp. 2286–2291, 2009.
- [37] M. N. Khorrami and E. G. Larsson, "Cooperative transmission based on decode-and-forward relaying with partial repetition coding," *IEEE Trans. Commun.*, vol. 8, no. 4, pp. 1716–1725, 2009.
- [38] Ö. Özdogan, E. Björnson, and E. G. Larsson, "Intelligent reflecting surfaces: Physics, propagation, and pathloss modeling," *IEEE Wireless Commun. Lett.*, 2020.
- [39] R. Karasik, O. Simeone, M. D. Renzo, and S. S. (Shitz), "Beyond Max-SNR: Joint encoding for reconfigurable intelligent surfaces," *CoRR*, vol. abs/1911.09443, 2019.
- [40] E. Björnson, Ö. Özdogan, and E. G. Larsson, "Intelligent reflecting surface vs. decode-and-forward: How large surfaces are needed to beat relaying?" *IEEE Wireless Commun. Lett.*, vol. 9, no. 2, pp. 244–248, 2020.